Korean J. Chem. Eng., 40(6), 1331-1339 (2023)
DOI: 10.1007/s11814-022-1375-x

pISSN: 0256-1115
eISSN: 1975-7220

Controllable synthesis of bowl-shaped porous carbon materials through didodecyldimethylammonium bromide for high performance supercapacitors

Qian Guo*,‡, Bingyu Li*,‡, Ming Shen*,†, Weizheng Li*, Qiang Gao*, and Guodong Xu,†**

*College of Chemistry and Chemical Engineering, Yangzhou University, Yangzhou, Jiangsu 225002, P. R. China
**School of Chemistry and Environmental Engineering, Yancheng Teachers University, Yancheng 224007, P. R. China
(*Received 7 August 2022 • Revised 25 November 2022 • Accepted 11 December 2022*)

Abstract−A series of bowl-shaped porous carbon materials was successfully synthesized by the use of didodecyldimethylammonium bromide as the soft template agent. By controlling the dosage of the soft template agent and the water/ethanol ratio of the solvent, the size and structure of the carbon materials can be precisely controlled. The prepared carbon materials with stacked bowl structure have good specific surface area (1,380.20 m^2 g^{-1}), large pore volume (1.27 cm^3 g^{-1}) and high heteroatom N doping amount (6.68 at.%). Moreover, electrochemical tests in 6 M KOH demonstrated impressive electrochemical performance, where the specific capacity of the typical materials was measured to be 191.0 F g^{-1} (at the current density of 1 A g^{-1}), and the capacity retention rate of typical materials was 80% (at the current density of 10 A g^{-1}).

Keywords: Porous Carbon Materials, Didodecyldimethylammonium Bromide, Cationic Surfactants, Bowl Structure, Supercapacitors

INTRODUCTION

Porous hollow carbon spheres have been widely studied and utilized as a kind of electrode material for electrochemical energy storage devices. Porous hollow carbon spheres have unique advantages associated with their structures and properties, such as internal cavity availability, thermal stability, chemical stability, high specific surface area, adjustable size, controllable pore structure and surface modification function [1-3]. These advantages allow hollow porous carbon spheres to play an important role in electrochemical energy storage devices, and especially in double layer supercapacitors. The most commonly used method for the synthesis of porous carbon materials is the template method, which can be divided into hard template method and soft template method. The hard template method uses hard template agents with certain three-dimensional structure (e.g., silica nanoparticles, polystyrene spheres, metal oxides, etc.) by coating with the precursor containing carbon in the synthesis of carbon materials [4,5]. After reaction under desired conditions, materials with rich pore structure are obtained followed by centrifugation, drying, carbonization, etching and other post-treatment steps to remove the hard template. Cao et al. synthesized a cobalt benzimidazole framework (ZIF-9) derived carbon composite with a unique quasi-microcubic morphology and used the as-prepared materials as an electrode material for the CDI [6]. Although the hard template method is simple to operate, it is easy to destroy the material structure and introduce impurity atoms in the process of removing the template, which has certain limitations. The soft template method is based on the organic self-assembly of thermosetting carbon precursors and thermal decomposition of amphiphilic molecules (such as surfactants, block polymers) to form ordered porous hollow carbon spheres. Therefore, compared with the hard template method, the soft template method can easily control the shape size, the cavity wall thickness and the aperture structure of the carbon spheres [7-9]. It can be seen that the key to the soft template method is the selection and adjustment of soft template agent. The carbon precursors and amphiphilic molecules in soft template method are often polymerized at low temperature. The common carbon precursors [10] usually include benzene, phenol, ethylene, resorcinol, formaldehyde, dihydroxybenzoic acid, coke, polystyrene, polyacrylonitrile and so on, most of which are fossil-based chemicals. These carbon precursors are generally toxic to a certain degree and are not cheap. Therefore, it is necessary to select the optimal soft template in the process of synthesis to obtain the ideal results and to ensure environmental sustainability at the same time. There are numerous studies on the synthesis of porous hollow carbon spheres by soft template method. Li et al. successfully fabricated nitrogen-doped mesoporous graphitized carbon nano-materials using Gemini cationic surfactants as a soft template [11]. Li et al. achieved the controlled synthesis of single carbon nanospheres to three-dimensional carbon skeleton by using bis-decyl dimethyl ammonium bromide as a soft template agent, and successfully prepared three-dimensional carbon framework electrode material with interconnected pore structure inside the shell layer for excellent performance of supercapacitor [12]. Jia et al. synthesized a series of nitrogen-doped porous carbon spheres by polymerization of 3-aminophenol with amphiphilic aliphatic aldehydes using imidazole-type cationic surfactants as a soft template [13]. Song et al. designed a simple synthetic route to obtain carbon hydrangeas integrated with unique geometry, high surface areas, N/O doping, and well-developed pore

†To whom correspondence should be addressed.
E-mail: shenming@yzu.edu.cn, xuguodong003@gmail.com
‡These authors contributed equally to this work.

structure [14]. Moreover, the use of typical surfactant cetyltrimethylammonium bromide (CTAB) opens the door to the regulation of porous hollow carbon spheres, and didodecyldimethylammonium bromide (DDAB) has a more specific structure than CTAB and didecyldimethylammonium bromide. Cationic surfactant DDAB has a hydrophilic head group and two hydrophobic chains. Compared with traditional surfactants and block copolymers, the ordered combination of DDAB has more unique microstructure. DDAB is composed of two longer hydrophobic chains and a hydrophilic headgroup, and the relatively strong interaction force between the hydrophobic chains facilitates the formation of a soft template for unique structure, thus facilitating the formation of bowl carbon spheres with interconnected pores of the shell.

In this work, a series of porous carbon micro/nanospheres (PCMNSs) with the stacked bowl structure was successfully achieved by the use of DDAB as the soft template agent. What is more, by adjusting the dosage of the soft template agent and water/ethanol ratio of the solvent, the size and structure of the carbon materials can be precisely controlled. The bowl carbon spheres have the same or even better specific surface area than the porous hollow carbon spheres because of their small volume and stackability [10]. Compared with the porous hollow carbon sphere, the stacking of bowl-shaped structure and bowl-shaped structure significantly improves the availability of material space, so the bulk density in the limited space of the bowl carbon spheres has been markedly improved. These morphological and structural advantages allow the bowl structure carbon spheres to have a high volume specific capacity with the bowl structure carbon spheres as the electrode materials. At the same time, the bowl structure carbon spheres therefore may have a good application prospect in sensing and biomedicine because of its open arc structure [15,16].

EXPERIMENTAL SECTION

1. Materials

3-Aminophenol, anhydrous ethanol, ethyl orthosilicate (TEOS) and potassium hydroxide (KOH) were all analytically pure and supplied by Sinophenol Chemical Reagent Co., LTD. DDAB, formaldehyde solution (37-40 wt%), hydrofluoric acid solution (40 wt%), polytetrafluoroethylene dispersions (60 wt%), ammonia solution (25-28 wt%) and acetylene black were provided by Shanghai Aladdin Biochemical Technology Co., LTD. Nickel foam and diaphragm were supplied by Cyber Electrochemical Materials Network. The water was deionized and made from laboratory instruments.

2. Preparation of PCMNSs

The preparation process of PCMNSs is shown in Fig. 1. Deionized water (50 mL), anhydrous ethanol (6-15 mL) and 3-aminophenol (0.6 g) were successively added to the round-bottom flask with intense stirring at 30 °C (300 r min^{-1}), and the soft template DDAB (0.6-1.2 g) was added after the 3-aminophenol was slowly dissolved for about ten minutes. When DDAB was completely dissolved, an ammonia solution (0.6 mL) was added to the above mixture. After 20 minutes, the formaldehyde solution (0.84 mL) was added to the mixture. As the reaction progressed, TEOS (3 mL) was added immediately when white precipitates began to appear in the mixed solution. After all reactants had been added, the mixture was stirred at constant temperature for 24 hours. After the reaction, the solution was transferred to the reactor and placed in a 100 °C constant temperature drying oven for 24 hours. After natural cooling, the products were collected by centrifugation, washed alternately with water and ethanol, and freeze-dried. In a tubular furnace (nitrogen atmosphere), at 1 °C min^{-1}, the sample was treated under a heat-

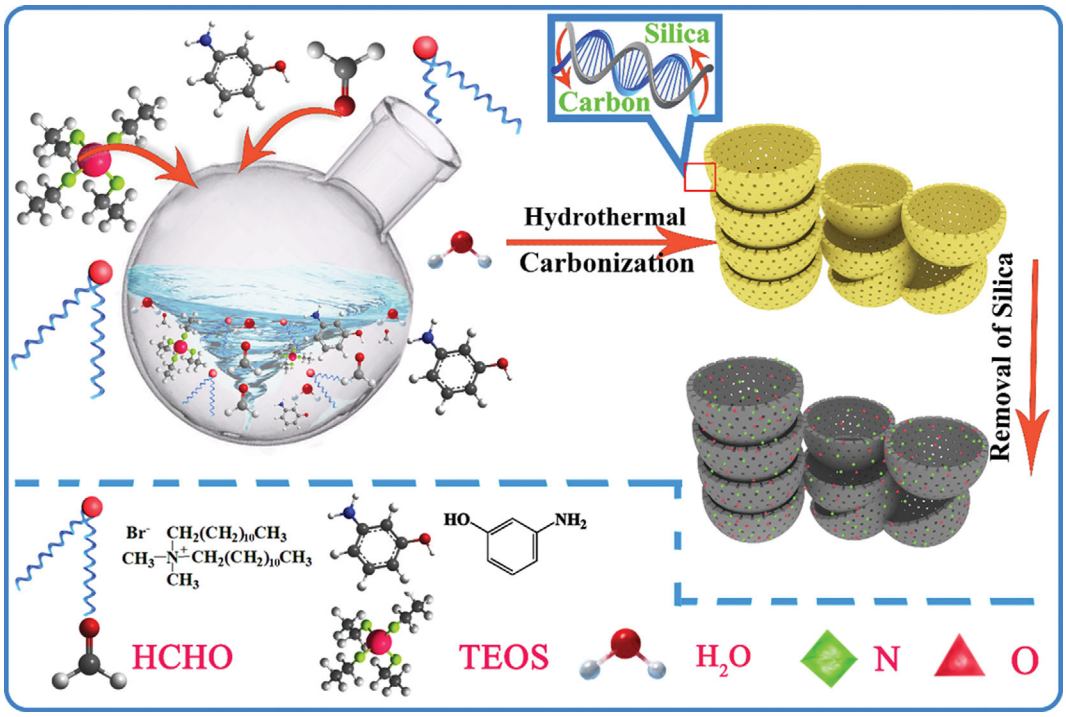

Fig. 1. Schematic diagram of the preparation of stacked bowl-shaped carbon spheres.

ing rate of 350 °C for two hours and under the same heating rate at 850 °C for carbonization. After carbonization, the product was etched with 20% HF for 48 hours, dried and collected. The porous carbon microspheres synthesized by the above method were named PCMNSs-M-N, where M represents the mass of surfactant (g) and N represents the volume of anhydrous ethanol (mL).

3. Characterization

Field emission scanning electron microscopy (FE-SEM) images of PCMNSs prepared by employing surfactants with two hydrophobic chains were conducted on Hitachi S-4800II. Transmission electron microscopy (TEM) images were carried out on Netherlands Philips Tecnai 12. An X-ray diffractometer (AXS D8 Advance, Bruker) and a Raman spectrometer (In Via, Renishaw) were used for powder X-ray diffraction (XRD) and Raman spectra. The content of heteroatom in the product was determined by XPS spectra (ESCALAB 250Xi, Thermo Fisher Scientific). The corresponding EDX elemental mapping was conducted to explore the element composition and distribution of the prepared materials. Pyrene was used as a fluorescence probe to detect 3-aminophenol with different molar concentrations in the solution of didecyldimethylammonium bromide surfactant, water and ethanol by fluorescence spectrophotometer (F-7000).

4. Electrochemical Measurements

The electrochemical performance of PCMNSs was tested in a double-electrode electrochemical system with 6 M KOH electrolyte at CHI760E electrochemical workstation of Shanghai Chenhua instrument. The cyclic voltammetry curve, galvanostatic charge discharge curve and AC impedance spectrum of carbon-based material PCMNSs were obtained. The working electrode was prepared by pressing a homogeneous slurry of carbon sample 0.08 g (85 wt%), acetylene black 0.0094 g (10 wt%), and 0.0078 g polytetrafluoroethylene (5 wt%) on nickel foam current collector, then dried at 105 °C for 1 h. Finally, then soaked in the electrolyte solution for ten hours. The active area of the working electrode was 95.033 mm^2 and the film thickness of the sample was 0.042 mm. Foam nickel and polypropylene film were used as a collector and an isolator of EDLCs, respectively. The specific capacitances of carbon-based materials were calculated by the equation:

$$C_g = \frac{2I}{(dV/dt)m}$$

where C_g (F g^{-1}) is the specific capacitance of a single electrode, I (A) is the discharge current, m (g) is the mass of a single electrode, while dV/dt (V s^{-1}) is the slope of the discharge curve after the voltage drop.

RESULTS AND DISCUSSION

A series of nitrogen-doped porous carbon materials with different micromorphology were synthesized by the one-step sol-gel method with varying chain length of hydrophobic chain of soft template agent. FE-SEM images (Fig. 2) show that the prepared PCMNSs have controllable size and morphology. By changing the template structure of the emulsion interface microreactor, monodispersed carbon spheres and stacked open carbon bowl carbon spheres were synthesized successfully. The same results can be confirmed by TEM of the prepared PCMNSs (Fig. 3). From Fig. 2 and Fig. 3, it can be seen that the size of carbon materials can be precisely controlled by adjusting the amount of ethanol. When the dosage of DDAB as the soft template was kept unchanged, the size of the monodisperse carbon nanospheres gradually increased with the increase of the amount of ethanol. The average particle sizes of PCMNSs-0.6-6, PCMNSs-0.6-10 and PCMnSs-0.6-15 were 200 nm, 225 nm and 570 nm, respectively. When the amount of soft template was 1.2 g, the carbon material changed from monodispersed carbon sphere structure to stacked bowl structure with the increase of the amount of ethanol, and the average diameter of carbon bowl gradually increased. The average diameter of the carbon bowl of PCMNSs-1.2-6, PCMNSs-1.2-10 and PCMNSs-1.2-15 was 220 nm, 250 nm and 1,280 nm, respectively. The bowl-shaped structure of PCMNSs-1.2-6 contributes to higher bulk density and specific surface area of the material. The rice flower structure of PCMNSs-

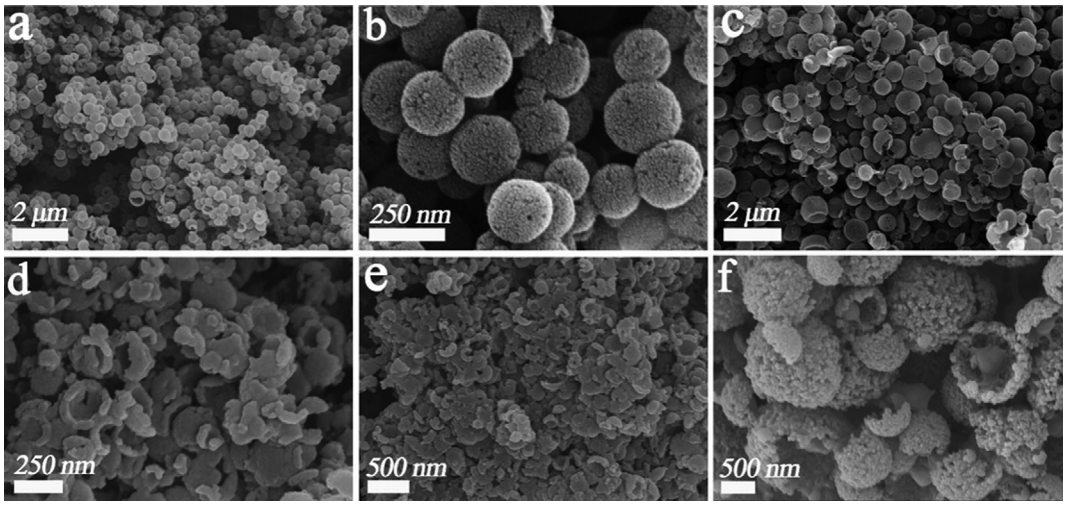

Fig. 2. SEM images of PCMNSs: (a) PCMNSs-0.6-6; (b) PCMNSs-0.6-10; (c) PCMNSs-0.6-15; (d) PCMNSs-1.2-6; (e) PCMNSs-1.2-10; (f) PCMNSs-1.2-15.

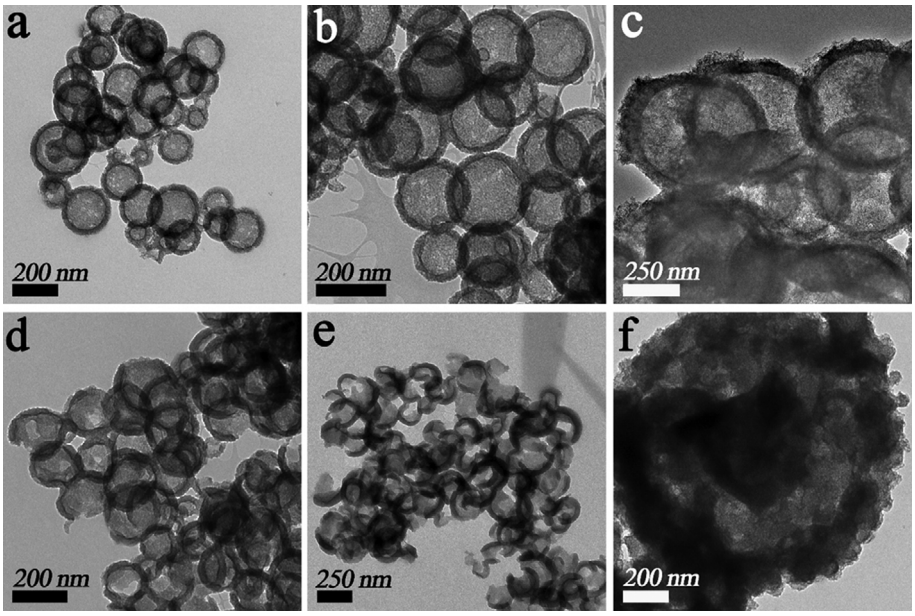

Fig. 3. TEM images of PCMNSs: (a) PCMNSs-0.6-6; (b) PCMNSs-0.6-10; (c) PCMNSs-0.6-15; (d) PCMNSs-1.2-6; (e) PCMNSs-1.2-10; (f) PCMNSs-1.2-15.

1.2-15 with the abundant pores on the surface is conducive to the rapid ion transport in the electrolyte [17].

When the amount of ethanol was fixed, and by increasing dosage of surfactant, the average particle sizes increased while the morphology of the carbon materials changed to an open structure. Because of the increasing of surfactant amount, the micelle aggregation number of surfactant increased, and the resulting soft template structure was larger. After the post-treatment process, such as high-temperature calcination and etching, the carbon spheres with larger average particle size were therefore formed. Compared with the carbon nanospheres or carbon nanotubes, the bowl carbon spheres had better ionic wetting of electrolyte, lower charge transfer resistance and better electrochemical conductivity [17,18]. From Fig. 2 and Fig. 3, there are abundant pore structures between the carbon spherical shells, and these pore structures show different pore size distribution, which potentially provides high-quality transport channels for electrolyte ion transport.

According to the mesostructures of the prepared materials and the research results of predecessors [19,20], a possible synthesis mechanism of bowl-shaped carbon spheres is proposed and demonstrated as follows. When the surfactant was added to the reaction system, the DDAB with two hydrophobic chains and one hydrophilic head group self-assembled to form micellar structures in a mixed solution of water and ethanol. Because of the membrane strength of the DDAB micellar was weak, it was easy to cross link and fuse with the adjacent micelles to form a three-dimensional molecular ordered assembly. 3-aminophenol compatibilized to the hydrophobic core of the surfactant as the reaction proceeded. After ammonia and formaldehyde were added to the system, 3-aminophenol reacted with formaldehyde between the interface of the surfactant. Ammonia was used as catalyst in the condensation reaction to produce a large number of hydroxymethyl substitutes in the mixture of water and ethanol. When the silicate anion hydrolyzed by TEOS met the positive cationic surfactant of DDAB, the strong electrostatic interaction formed a unique soft template structure. DDAB has a hydrophilic group and two hydrophobic chains, and the hydro-

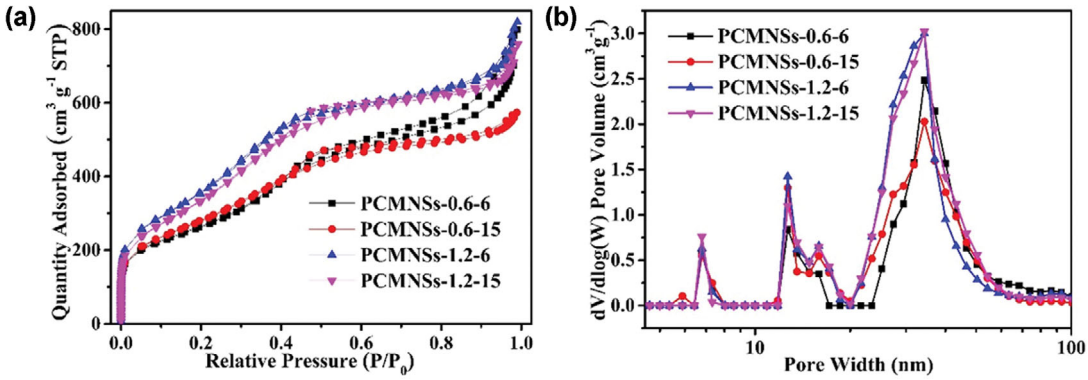

Fig. 4. (a) The N_2 adsorption-desorption isotherms of PCMNSs; (b) Pore size distribution curve of PCMNSs.

Table 1. Specific surface area and pore structure parameters of PCMNSs

Samples	S_{BET} (m^2 g^{-1})	Pore volume (cm^3 g^{-1})			
		V_{total}	$V_{micropore}$	$V_{mesopore}$	$V_{macropore}$
PCMNSs-0.6-6	961.26	1.24	0.12	1.02	0.10
PCMNSs-0.6-15	1,025.81	0.89	0.17	0.70	0.02
PCMNSs-1.2-6	1,380.20	1.27	0.19	1.02	0.06
PCMNSs-1.2-15	1,272.62	1.18	0.18	0.94	0.06

Notes: S_{BET} represents the specific surface area of the sample; V_{total} represents the total pore volume of the sample; $V_{micropore}$ represents the volume of the hole whose hole size is less than 2 nm; $V_{mesopore}$ represents the volume of the hole with a hole size between 2-50 nm; $V_{macropore}$ represents the volume of a hole with a hole size greater than 50 nm.

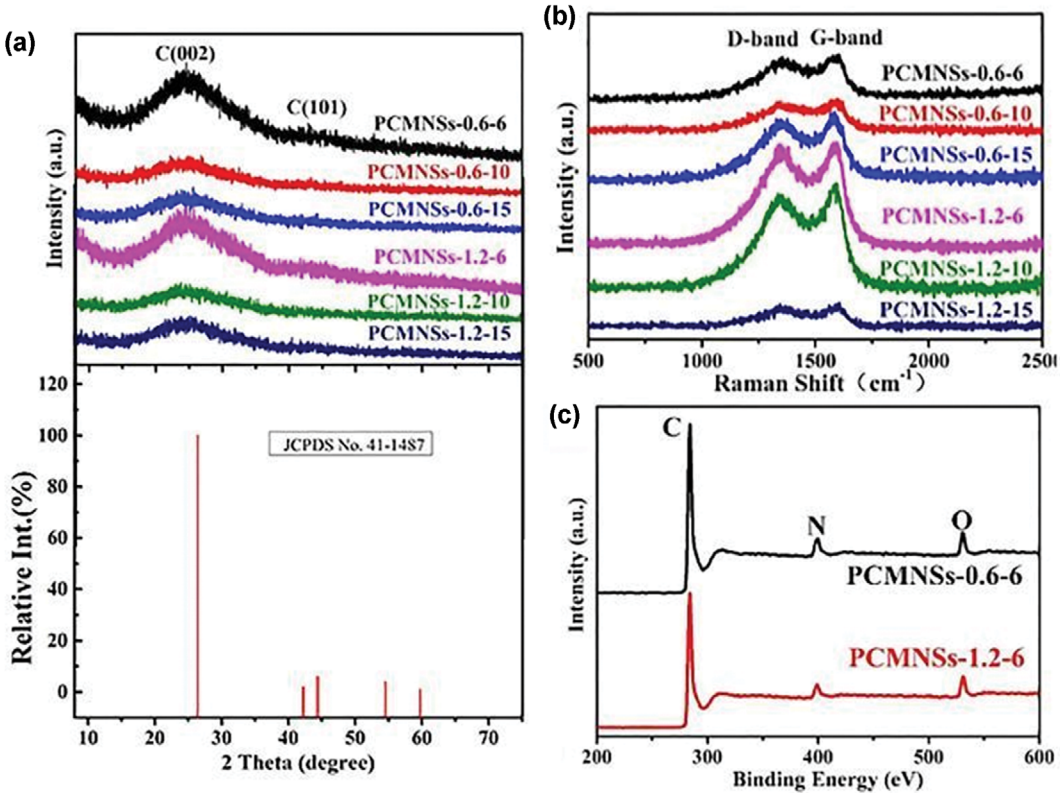

Fig. 5. (a) XRD pattern of PCMNSs; (b) Raman spectra of PCMNSs; (c) XPS full spectrum of PCMNSs.

phobic chains of DDAB are longer. The greater length of hydrophobic chains reduced the film strength of the surfactant micelles, which formed a unique bowl soft template structure. The carbon materials with bowl-shaped structure were successfully produced after calcination. The synthesis mechanism diagram is shown in Fig. S1.

The N_2 adsorption-desorption isotherms of the PCMNSs (Fig. 4(a)) exhibit typical type-IV hysteresis [21], where the pore size distribution image (Fig. 4(b)) can indicate that PCMNSs has a unique hierarchical pore structure. The micropores (<2 nm) are mainly derived from the thermal decomposition of phenolic resin during high temperature carbonization. The mesopores (2-50 nm) are associated with the thermal decomposition of DDAB and the removal of silica, and meso-macropores (>50 nm) originate from the hollow part of carbon spheres or the clearance between the materials. The specific surface area and pore volume of PCMNSs-0.6-6, PCMNSs-0.6-15, PCMNSs-1.2-6 and PCMNSs-1.2-15 were measured to be 961.26, 1,025.81, 1,380.20, 1,272.62 m^2 g^{-1} and 1.24, 0.89, 1.27 and 1.18 cm^3 g^{-1}, respectively (Table 1). The PCMNSs-1.2-6 with uniform open structure had the largest specific surface area and pore volume, which can provide large available area and fast transport channel for effective electrolyte ion transport [22,23]. The large pore and open structure of PCMNSs-1.2-6 facilitate the mass transfer process of electrolyte ions, while the mesoporous and micropores provide higher specific surface area and abundant active sites.

The physical structure and graphitization degree of PCMNSs were characterized by XRD and Raman spectroscopy. As demonstrated in Fig. 5(a), the XRD patterns of PCMNSs have two broad characteristic diffraction peaks at about 23.5° and 44.6°, which correspond to the (002) and (101) crystal planes of disordered carbon,

respectively [24,25]. Raman spectra (Fig. 5(b)) show that PCMNSs have a relatively wide D-band at 1,342.8 cm^{-1} and a relatively narrow G-band at 1,596.9 cm^{-1}. The D band originates from the vibrations of disordered carbon or the defects in the plane terminations, and the G band is related to the vibrations of ordered sp^2-bonded graphitic carbon sheets [26,27]. The peak intensity ratio of the D band to the G band (I_D/I_G) is calculated to be 0.89-0.98 in Table S1, which implies that PCMNSs has a high graphitization degree and a large number of amorphous carbon structure defects. In wide-scan XPS spectra (Fig. 5(c)), the featured peaks of C 1s (285.7 eV), N 1s (399.9 eV) and O 1s (531.5 eV) appear, respectively, indicating that N atoms had been successfully introduced into the structure of PCMNSs [28]. Table S2 lists the contents of N, C and O elements in the PCMNSs. The N content of PCMNSs-0.6-6 is 7.37 at.%, which indicates that the use of 3-aminophenol and DDAB has achieved high proportion of in situ nitrogen atom self-doping. The high-resolution N 1s spectra of PCMNSs (Fig. S2) show that there were four forms of N in PCMNSs: pyridine nitrogen (N-6, 398.3 eV), pyrrole nitrogen (N-5, 399.8 eV), graphite nitrogen (N-Q, 401.0 eV) and nitrogen oxide (N-4, 402.6 eV). These results indicate that the N element had been successfully doped into the structure of carbon [29]. The element mapping diagram of PCMNSs-1.2-6 (Fig. 6)

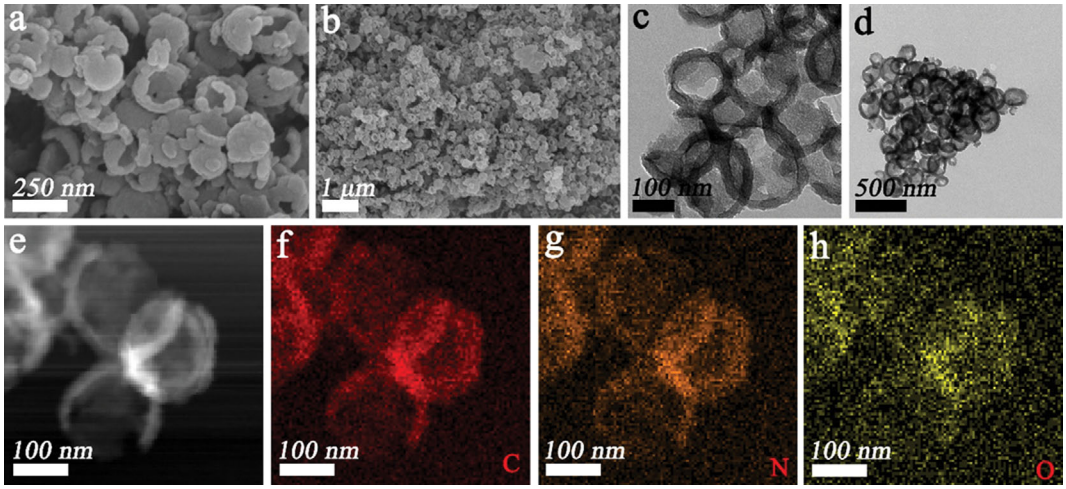

Fig. 6. PCMNSs-1.2-6 (a, b) FE-SEM; (c, d) TEM; (e) High resolution transmission electron microscope images; (f, g, h) corresponding mapping of carbon, nitrogen and oxygen elements.

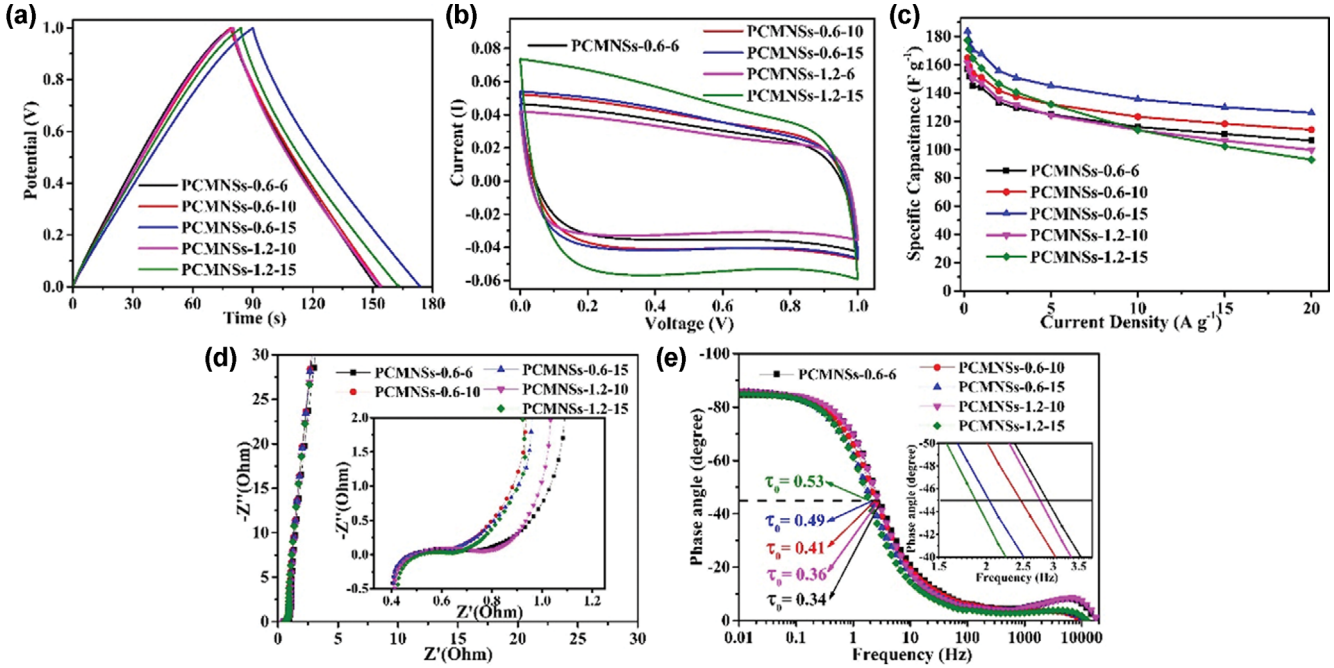

Fig. 7. Electrochemical test results of PCMNSs-0.6-6, PCMNSs-0.6-10, PCMNSs-0.6-15, PCMNSs-1.2-10 and PCMNSs-1.2-15 in a symmetrical two-electrode system: (a) Current-constant charge-discharge curves (1 A g^{-1} Current density); (b) Cyclic voltammetry curve (500 mV s^{-1} Scanning rate); (c) Specific capacity curve; (d) Nyquist diagram; (e) Potter figure.

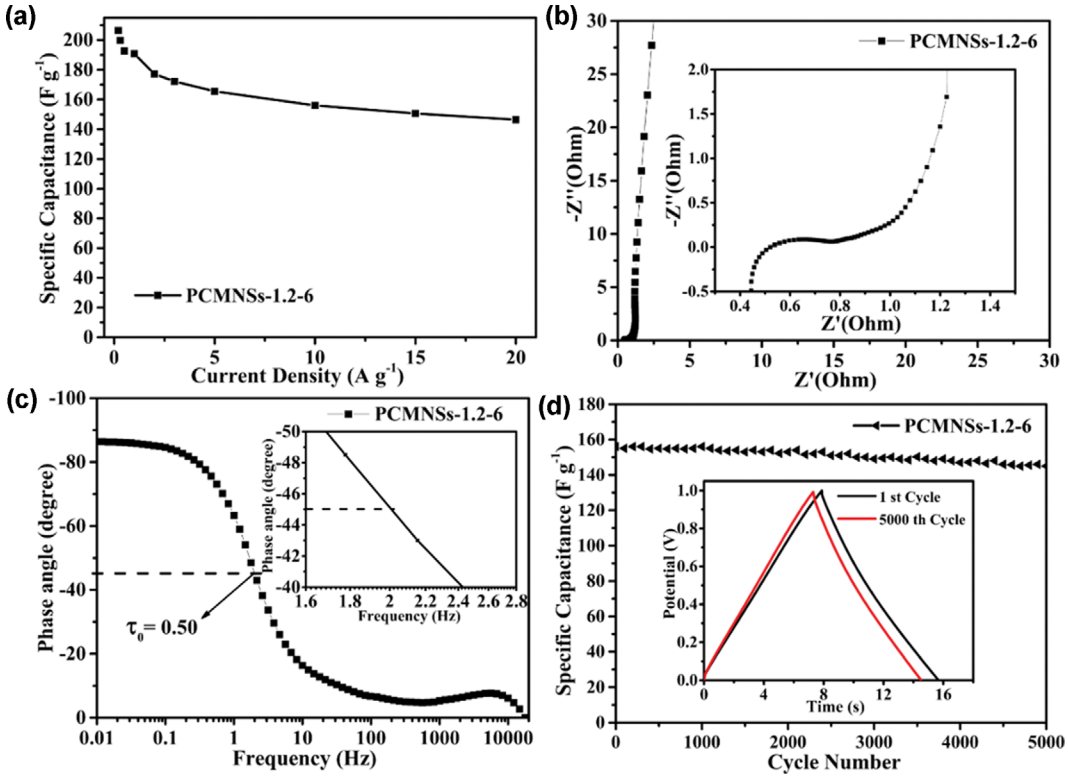

Fig. 8. (a) Specific capacity curve of stacked bowl-shaped carbon spheres PCMNSs-1.2-6; (b) Nyquist diagram; (c) Bode diagram; (d) Long-term cyclic stability (10 A g^{-1}, 5000 cycles at current density).

shows that C, N and O elements are evenly distributed in the skeleton structure of carbon [30].

PCMNSs based electrode materials demonstrated high electrochemical capacitive reversibility [31,32]. (Galvanostatic charge-discharge curves of PCMNSs at 1 A g^{-1} (Fig. 7(a)) show almost isosceles triangles.) As demonstrated in Fig. 7(b), PCMNSs display symmetrical rectangular CV curves at a scan rate of 500 mV s^{-1}, indicating the typical electrical double layer capacitive properties of energy storage [33]. According to the charge-discharge curves of constant current, the electrochemical specific capacities of all samples under different current densities were calculated and listed in Table S3. The specific capacity of PCMNSs-0.6-6, PCMNSs-0.6-10, PCMNSs-0.6-15, PCMNSs-1.2-6, PCMNSs-1.2-10 and PCMNSs-1.2-15 was measured to be 145.8, 151.0, 167.6, 191.0, 147.2 and 157.6 F g^{-1}, respectively (at the current density of 1 A g^{-1}). The calculated energy densities are 5.06, 5.24, 5.82, 6.63, 5.11 and 5.47 Wh kg^{-1}, respectively (Table S4). The representative samples of PCMNSs-1.2-6 with stacked bowl structure show the best supercapacitor energy storage performance (Fig. S3(b) and S3(c)). At the current densities of 0.2, 0.3, 0.5, 1, 2, 3, 5, 10, 15, 20, 30, 40 and 50 A g^{-1}, the PCMNSs-1.2-6 displays the highest specific capacity of 206.4, 199.2, 192.8, 191.0, 177.2, 172.2, 165.5, 156.0, 150.6, 146.4, 139.9, 134.3 and 128.9 F g^{-1}, respectively. The specific capacity reached 206.4 F g^{-1} at the current density of 0.2 A g^{-1} and its energy density was 7.17 Wh kg^{-1}. Compared to low current density 1 A g^{-1}, the capacity retention rate of the PCMNSs reached 76.6% at high current density 20 A g^{-1} and 67.5% at ultra-high current density 50 A g^{-1}. The stacked bowl structure of PCMNSs has the best electrochemical performance, because the stacked open carbon bowls can shorten the diffusion path which can limit the ion migration in the electrolyte [31].

PCMNSs based electrode materials show excellent stability and low energy density attenuation at high current density (Fig. 7(c) and 8(a)). Among all the samples, the specific capacity of PCMNSs-1.2-15 decreased the fastest with the increase of current density, as the large diameter of PCMNSs-1.2-15 suggests the longest electrolyte ion diffusion distance, which reduces the diffusion efficiency of PCMNSs [34]. The stacked bowl-shaped structure of PCMNSs provides higher capacity while maintaining the optimal ratio performance (Fig. 8(a)). At the current density of 10 g A^{-1}, the specific capacity retention rate of PCMNSs-1.2-6 with stacked bowl-shaped structure was 93% after 5000 cycles of current density (Fig. 8(d)), showing excellent long cycle stability. The electrochemical impedance spectrum of all PCMNSs electrodes shows nearly vertical lines (Fig. 7(d) and Fig. 8(b)) in the low frequency areas; the results indicated typical double-layer electrochemical capacitive behavior of PCMNSs [32,35]. Fig. S4 is the Nyquist plots of PCMNSs-1.2-6 electrodes after 5000 cycles. The interconnecting pore structure, super high specific surface area and large pore volume in the stacked bowl structure can significantly improve the electrochemical conductivity of the materials, and effectively improve the transfer efficiency of the electrolyte. The short time constant τ_0 of the PCMNSs-based electrode materials can be seen in Fig. 7(e) and Fig. 8(c), which indicates that the prepared electrodes have fast charging and discharging performance. The excellent electrochemical energy storage performance mainly comes from the stacked bowl hemi-

sphere of carbon. The stacked bowl-shaped structure not only improves the accumulation of material density, but also reduces the distance of pore structure between carbon bowl and other carbon bowl, which effectively facilitated electrolyte ion transport.

CONCLUSIONS

A series of hollow porous carbon materials was successfully synthesized by the use of DDAB as the soft template agent. By adjusting the amount of soft template agent and the solvent ratio of water/ethanol, the size and structure of the carbon material can be precisely controlled. Among the carbon materials, compared with the porous hollow carbon nanospheres, the stacked bowl carbon spheres (PCMNSs-1.2-6) have better specific surface area (1,380.20 $m^2 g^{-1}$), larger pore volume (1.27 $cm^3 g^{-1}$) and higher heteroatom N doping amount (6.68 at.%). The unique structural advantages provide more effective active sites, which contributes to good electrochemical performance. The specific capacity of PCMNSs-1.2-6 was measured to be 191.0 F g^{-1} (at the current densities of 1 A g^{-1}), and the capacity retention rate of PCMNSs-1.2-6 was 80% (at the current density of 10 A g^{-1}).

ACKNOWLEDGEMENTS

We acknowledge financial support from National Natural Science Foundation of China (Nos. 51907173, 21504033, 21673201), Top-notch Academic Programs Project of Jiangsu Higher Education Institutions, China (TAPP). We also acknowledge the Priority Academic Program Development of Jiangsu Higher Education Institutions, China.

CRediT AUTHORSHIP CONTRIBUTION STATEMENT

Qian Guo: Methodology, Investigation, Formal analysis, Writing-review & editing. **Bingyu Li:** Investigation, Formal analysis, Writing-review & editing. **Ming Shen:** Conceptualization, Methodology, Writing-review & editing. **Weizheng Li:** Investigation, Formal analysis, Writing-review & editing. **Qiang Gao:** Resources, Supervision, Writing-review & editing. **Guodong Xu:** Resources, Supervision, Writing-review & editing.

DECLARATION OF COMPETING INTEREST

The authors declare that they have no known competing financial interests or personal relationships that could have appeared to influence the work reported in this paper.

SUPPORTING INFORMATION

Additional information as noted in the text. This information is available via the Internet at http://www.springer.com/chemistry/journal/11814.

REFERENCES

1. Y. P. Zhai, Y. Q. Dou, D. Y. Zhao, P. F. Fulvio, R. T. Mayes and S. Dai, *Adv. Mater.*, **23**, 4828 (2011).
2. S. A. Shah, D. Kulhanek, W. M. Sun, X. F. Zhao, S. Yu, D. Parviz, J. L. Lutkenhaus and M. J. Green, *J. Colloid Interface Sci.*, **560**, 581 (2020).
3. R. Liu, S. M. Mahurin, C. Li, R. R. Unocic, J. C. Idrobo, H. J. Gao, S. J. Pennycook and S. Dai, *Angew. Chem. Int. Ed.*, **50**, 6799 (2011).
4. Z. L. Jian, S. Hwang, Z. F. Li, A. S. Hernandez, X. F. Wang, Z. Y. Xing, D. Su and X. L. Ji, *Adv. Funct. Mater.*, **27**, 1700324 (2017).
5. X. Y. Chen, C. Chen, Z. J. Zhang and D. H. Xie, *J. Mater. Chem. A*, **1**, 7379 (2013).
6. S. Cao, T. T. Chen, S. S. Zheng, Y. Bai and H. Pang, *Small Methods*, **5**, 2101070 (2021).
7. Z. G. Liang, L. M. Zhang, H. Liu, J. P. Zeng, J. F. Zhou, H. J. Li and H. Xia, *Results Phys.*, **12**, 1984 (2019).
8. F. F. Hu, Y. Lin, Y. Qiu, B. Wen, Y. N. Zheng and H. B. Yang, *Ceram. Int.*, **47**, 5968 (2021).
9. Y. Qin, L. Miao, M. Mansuer, C. M. Hu, Y. K. Lv, L. H. Gan and M. X. Liu, *ACS Appl. Mater. Interfaces*, **14**, 33328 (2022).
10. X. Liu, P. P. Song, J. H. Hou, B. Wang, F. Xu and X. M. Zhang, *ACS Sustain. Chem. Eng.*, **6**, 2797 (2018).
11. W. Z. Li, B. Y. Li, M. Shen, Q. Gao and J. H. Hou, *Chem. Eng. J.*, **384**, 123309 (2020).
12. B. Y. Li, Q. Guo, M. Shen, W. Z. Li and Q. Gao, *Micropor. Mesopor. Mater.*, **326**, 111379 (2021).
13. S. J. Jia, Q. Guo, M. Shen, Q. Gao and K. Wang, *Colloids Surf. A: Physicochem. Eng. Asp.*, **636**, 128064 (2022).
14. Z. Y. Song, H. Duan, L. Miao, L. Ruhlmann, Y. K. Lv, W. Xiong, D. Z. Zhu, L. C. Li, L. H. Gan and M. X. Liu, *Carbon*, **168**, 499 (2020).
15. W. Ma, Q. Zheng, Y. He, G. Li, W. Guo, Z. Lin and L. Zhang, *J. Am. Chem. Soc.*, **141**, 18271 (2019).
16. J. Y. Ma, Y. S. Zhang, X. H. Zhang, G. B. Zhu, B. Liu and J. H. Chen, *Talanta*, **88**, 696 (2012).
17. H. R. Wang, H. W. Zhou, M. Gao, Y. A. Zhu, H. T. Liu, L. Gao and M. X. Wu, *Electrochim. Acta*, **298**, 552 (2019).
18. C. C. Yang, W. T. Jing, C. Li and Q. Jiang, *J. Mater. Chem. A*, **6**, 3877 (2018).
19. M. Manousakis and A. Avranas, *J. Colloid Interface Sci.*, **402**, 237 (2013).
20. S. E. Friberg, H. Hasinović, Q. Yin, Z. Q. Zhang and R. Patel, *Colloids Surf. A: Physicochem. Eng. Asp.*, **156**, 145 (1999).
21. A. Mahmood, S. Li, Z. S. Ali, H. Tabassum, B. J. Zhu, Z. B. Liang, W. Meng, W. Aftab, W. H. Guo, H. Zhang, M. Yousaf, S. Gao, R. Q. Zou and Y. S. Zhao, *Adv. Mater.*, **31**, 1805430 (2019).
22. Y. X. Zhang, L. Liu, Y. F. Yu, Y. Zhang, S. L. Hou and A. B. Chen, *J. Phys. Chem. C*, **123**, 2801 (2019).
23. X. D. Yang, Y. L. Li, P. X. Zhang, L. N. Sun, X. Z. Ren and H. W. Mi, *Carbon*, **157**, 70 (2020).
24. H. R. Wang, J. Gao, J. Q. Zhu, J. Y. Ma, H. W. Zhou, J. Xiao and M. X. Wu, *Electrochim. Acta*, **334**, 135582 (2020).
25. X. Wu, Y. S. Si, Y. B. Zou, Y. T. Mao, Q. J. Li, S. X. Zhou, M. Chen and L. M. Wu, *ACS Appl. Mater. Interfaces*, **10**, 31664 (2018).
26. J. Du, Y. Zhang, H. X. Wu, S. L. Hou and A. B. Chen, *Carbon*, **156**, 523 (2020).
27. H. X. Qu, X. J. Zhang, J. J. Zhan, W. Q. Sun, Z. C. Si and H. K. Chen, *ACS Sustain. Chem. Eng.*, **6**, 7380 (2018).
28. D. F. Xue, D. Z. Zhu, W. Xiong, T. C. Cao, Z. W. Wang, Y. K. Lv, L. C.

Li, M. X. Liu and L. H. Gan, *ACS Sustain. Chem. Eng.*, **7**, 7024 (2019).
29. X. J. Zhang, S. J. Hou, Z. B. Ding, G. Zhu, H. R. Tang, Y. C. Hou, T. Lu and L. K. Pan, *J. Alloys Compd.*, **822**, 153578 (2020).
30. J. Ding, H. L. Zhang, H. Zhou, J. Feng, X. R. Zheng, C. Zhong, E. paek, W. B. Hu and D. Mitlin, *Adv. Mater.*, **31**, 1900429 (2019).
31. H. W. Zhang, O. Noonan, X. D. Huang, Y. N. Yang, C. Xu, L. Zhou and C. Z. Yu, *ACS Nano*, **10**, 4579 (2016).
32. D. Saha, Y. C. Li, Z. H. Bi, J. H. Chen, J. K. Keum, D. K. Hensley, H. A. Grappe, H. M. Meyer, S. Dai, M. P. Paranthaman and A. K. Naskar, *Langmuir*, **30**, 900 (2014).
33. A. Borenstein, O. Hanna, R. Attias, S. Luski, T. Brousse and D. Aurbach, *J. Mater. Chem. A*, **5**, 12653 (2017).
34. Z. Y. Song, L. Miao, L. C. Li, D. Z. Zhu, L. H. Gan and M. X. Liu, *Carbon*, **180**, 135 (2021).
35. K. Pourreza, N. B. Adeh and N. Mohammadi, *J. Energy Storage*, **30**, 101429 (2020).

Supporting Information

Controllable synthesis of bowl-shaped porous carbon materials through didodecyldimethylammonium bromide for high performance supercapacitors

Qian Guo*,‡, Bingyu Li*,‡, Ming Shen*,†, Weizheng Li*, Qiang Gao*, and Guodong Xu,†**

*College of Chemistry and Chemical Engineering, Yangzhou University, Yangzhou, Jiangsu 225002, P. R. China
**School of Chemistry and Environmental Engineering, Yancheng Teachers University, Yancheng 224007, P. R. China
(*Received 7 August 2022 • Revised 25 November 2022 • Accepted 11 December 2022*)

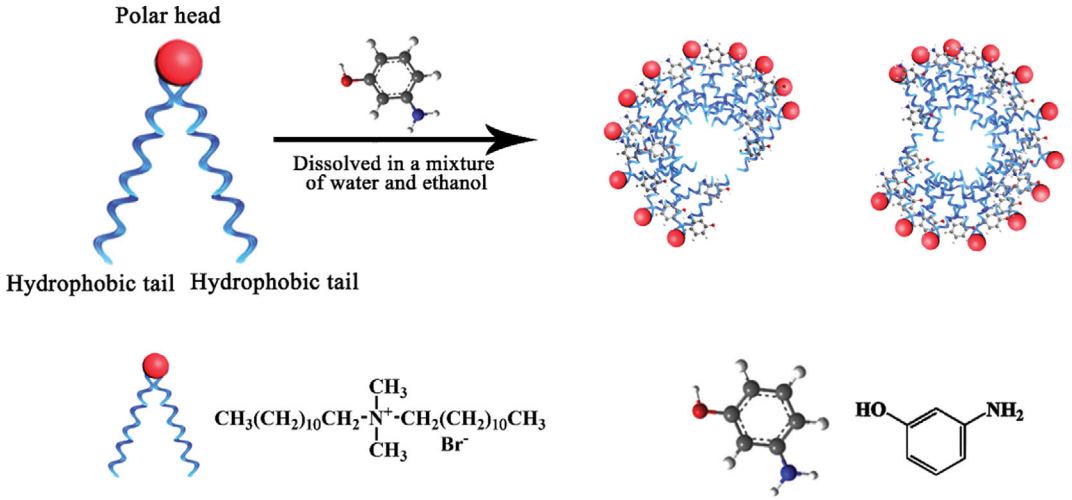

Fig. S1. Synthesis mechanism of open bowl-shaped carbon spheres.

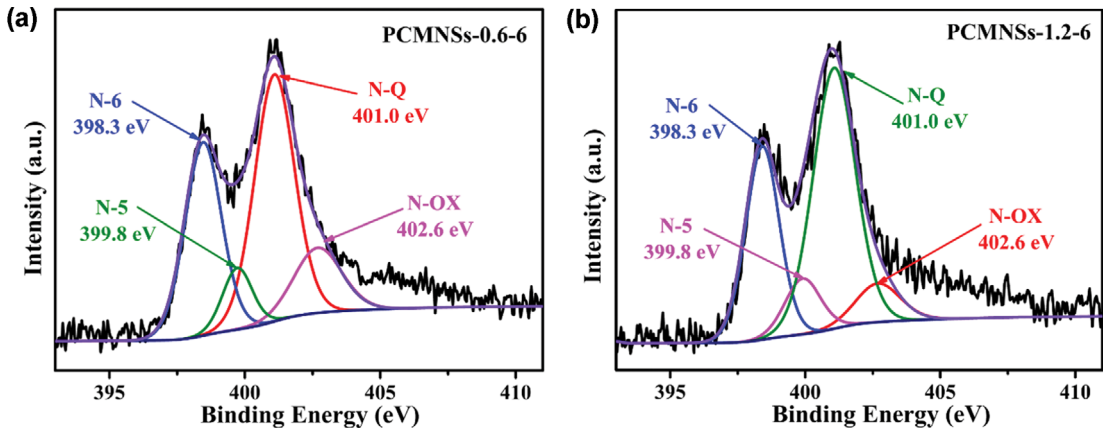

Fig. S2. High-resolution N 1s atlas (a) PCMNSs-0.6-6;(b) PCMNSs-1.2-6.

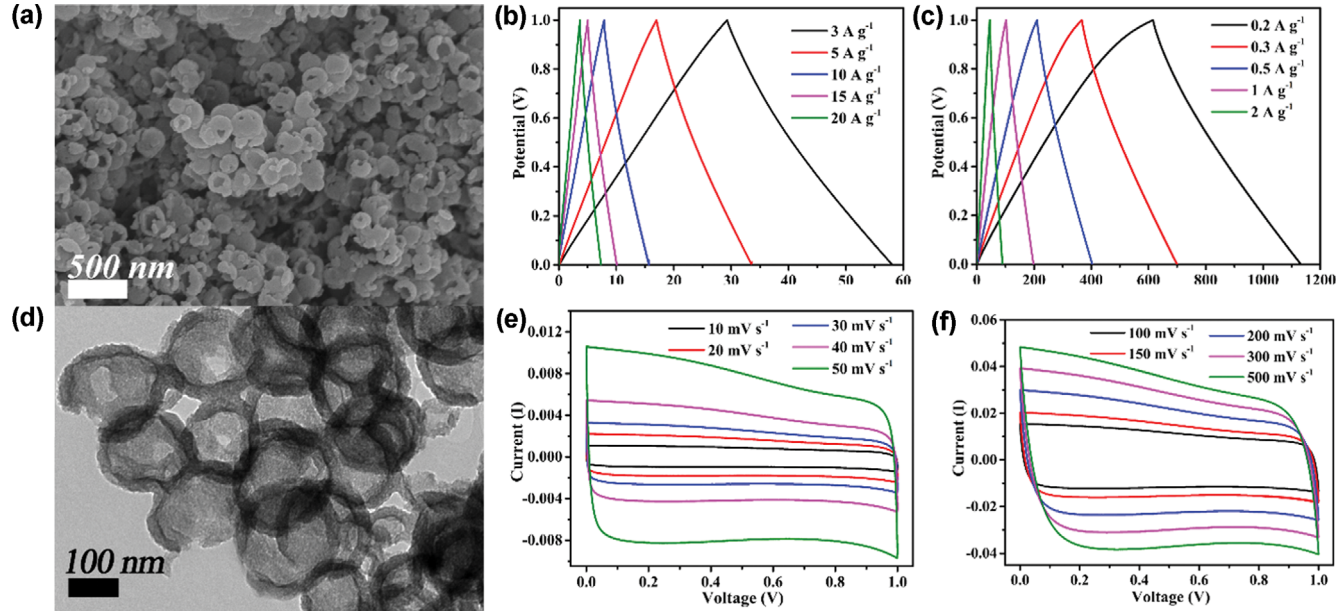

Fig. S3. Stacked open bowl-shaped carbon spheres PCMNSs-1.2-6 (a) SEM; (b), (c) Constant current charge-discharge curve (0.2-20 $A \cdot g^{-1}$ Current density); (d) TEM; (e), (f) cyclic voltammetry curve (10-500 $mV \cdot s^{-1}$ Scanning rate).

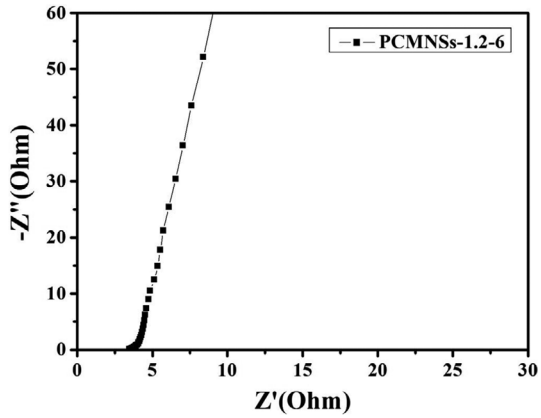

Fig. S4. Nyquist plots of stacked bowl-shaped carbon spheres PCMNSs-1.2-6 after 5000 cycles.

Table S1. Peak intensity ratio of THE D-band and g-band of PCMNSs (I_D/I_G)

Sample	I_D/I_G
PCMNSs-0.6-6	0.95
PCMNSs-0.6-10	0.91
PCMNSs-0.6-15	0.89
PCMNSs-1.2-6	0.98
PCMNSs-1.2-10	0.90
PCMNSs-1.2-15	0.94

Table S2. Elemental composition of PCMNSs and relative contents of different forms of nitrogen

Sample	N% (at.%)	C% (at.%)	O% (at.%)	N-6 (%) 398.3 eV	N-5(%) 399.8 eV	N-Q (%) 401.0 eV	N-OX (%) 402.6 eV
PCMNSs-0.6-6	7.37	80.31	4.69	14.69	22.51	53.55	9.24
PCMNSs-1.2-6	6.68	81.42	5.33	11.38	23.73	48.66	16.22

Table S3. Specific capacity of PCMNSs based electrodes at different current densities ($F \cdot g^{-1}$)

Sample	0.2 $A \cdot g^{-1}$	1 $A \cdot g^{-1}$	2 $A \cdot g^{-1}$	3 $A \cdot g^{-1}$	5 $A \cdot g^{-1}$	10 $A \cdot g^{-1}$	15 $A \cdot g^{-1}$	20 $A \cdot g^{-1}$
PCMNSs-0.6-6	157.6	145.8	133.6	129.7	123.9	116.0	111.0	106.3
PCMNSs-0.6-10	164.8	151.0	141.6	137.4	132.0	123.2	118.2	114
PCMNSs-0.6-15	183.6	167.6	155.6	150.7	145.1	135.6	129.9	126.0
PCMNSs-1.2-6	206.4	191.0	177.2	172.2	165.5	156.0	150.6	146.4
PCMNSs-1.2-10	161.2	147.2	135.6	131.5	124.2	113.8	106.2	99.76
PCMNSs-1.2-15	177.2	157.6	146.4	140.5	132.0	113.8	102.3	92.8

Table S4. Specific capacitances ($F \cdot g^{-1}$) and energy density ($Wh \cdot kg^{-1}$) of PCMNSs-based electrodes at 1 $A \cdot g^{-1}$ current densities

Sample	Specific capacitances at 1 $A \cdot g^{-1}$ ($F \cdot g^{-1}$)	Energy density ($Wh \cdot kg^{-1}$)
PCMNSs-0.6-6	145.8	5.06
PCMNSs-0.6-10	151.0	5.24
PCMNSs-0.6-15	167.6	5.82
PCMNSs-1.2-6	191.0	6.63
PCMNSs-1.2-10	147.2	5.11
PCMNSs-1.2-15	157.6	5.47